

## Supporting Information

# Non-oxidative dehydrogenation of methanol to dimethoxymethane over Ag/H $\beta$ zeolite bifunctional catalyst

Natalia Simitsis,<sup>a,b</sup> Felix Egger,<sup>c</sup> Mirijam Zobel,<sup>c,d</sup> Chalachew Mebrahtu<sup>a,b</sup> and Regina Palkovits<sup>a,b,†</sup>

<sup>a</sup> Institute for a Sustainable Hydrogen Economy, Forschungszentrum Jülich GmbH, 52428 Jülich, Germany.

<sup>b</sup> Chair of Heterogeneous Catalysis and Technical Chemistry, Institute for Technical and Macromolecular Chemistry, RWTH Aachen University, 52074 Aachen, Germany.

<sup>c</sup> Institute of Crystallography, RWTH Aachen University, Jägerstrasse 17–19, D-52066 Aachen, Germany.

<sup>d</sup> JCNS-3: Neutron Analytics for Energy Research, Forschungszentrum Jülich GmbH, Wilhelm-Johnen-Strasse, D-52428 Jülich, Germany.

† Corresponding author.

## 1 Experimental

### 1.1 Catalyst synthesis

A commercial NH<sub>4</sub> $\beta$  zeolite (SiO<sub>2</sub>/Al<sub>2</sub>O<sub>3</sub> = 25, abcr) was calcined at 550°C (10°C/min) for 5 h to yield H $\beta$  zeolite (a  $\beta$  zeolite with protons as counter ions). The H $\beta$  zeolite was then dealuminated following a previously optimized procedure,<sup>[1,2]</sup> where 3 g of the zeolite was stirred in 165 mL of 8 M HNO<sub>3</sub> (65%, CHEMSOLUTE®) at 80°C and 500 rpm for 16 h. After the dealumination step, the H $\beta$  zeolite was washed with 4 L of deionized water until it reached a neutral pH, then dried overnight at 110°C. Ag was loaded on the dealuminated H $\beta$  zeolite support using incipient wetness impregnation (IWI). The appropriate amount of AgNO<sub>3</sub> (>99.9%, Carl Roth) was dissolved in 0.5 mL of deionized water and added dropwise to 0.4 g of the H $\beta$  support, followed by manual stirring. The mixture was dried overnight at 80°C, then calcined at 450°C (5°C/min) for 3 h. The final catalysts are referred to as AgX/H $\beta$ , where X represents the Ag loading in wt.%.

### 1.2 Catalyst characterization

#### 1.2.1 ICP-OES (Inductively coupled plasma – optical emission spectroscopy)

The Ag loading was quantified based on ICP-OES on a kSPECTROBLUE device from SPECTRO Analytical Instruments GmbH. For these measurements, approx. 30 mg of the respective sample was added to a solution of conc. H<sub>2</sub>SO<sub>4</sub> (2 mL), diluted HF (8 mL) and H<sub>2</sub>O (40 mL) and the sample was digested by heating to 150°C in a microwave (600 W, 20 min). This solution was then diluted with distilled water and the ICP-OES measurement was performed.

#### 1.2.2 Powder X-ray diffractometry (XRD)

XRD measurements were carried out on a D2 PHASER XE-T device from Bruker. Cu-K $\alpha$  radiation ( $\lambda$  = 0.15406 nm) was used and measured in 2 $\theta$  angles from 6 – 90° in 0.02° steps.

#### 1.2.3 N<sub>2</sub>-physisorption

The N<sub>2</sub> adsorption and desorption isotherms of the calcined Ag/H $\beta$  catalysts were measured at -196 °C using a Quadrasorb SI unit from 3P Instruments. Prior to the measurement, the samples were evacuated for 6 h in a FloVac degasser at 150°C. The isotherms were analyzed using the QuadraWin software. The specific surface area S<sub>BET</sub> was determined using the Brunauer-Emmett-Teller (BET) method in the p/p<sub>0</sub> range of 0.05 – 0.2. The micropore volume was quantified using the t-plot model in the p/p<sub>0</sub> range of 0.2 – 0.4. The total pore volume was determined from the adsorbed N<sub>2</sub> volume at a p/p<sub>0</sub> ratio of 0.95.

#### 1.2.4 Thermogravimetric analysis (TG)

The TG of the calcined and spent Ag<sub>2</sub>O/H $\beta$  catalysts was carried out in air from 30 – 1000°C (5°C/min) using a “Netzsch STA 409” device.

#### 1.2.5 Temperature programmed reduction with H<sub>2</sub> (H<sub>2</sub>-TPR)

For the H<sub>2</sub>-TPR measurements, a ChemBet Pulsar TPR/TPD/TPO device from Quantachrome Instruments equipped with a thermal conductivity detector (TCD) was used. In a typical measurement, 30 mg of catalyst was first dried under He flow (22.4 mL/min) for 1 h at 150°C and then reduced in a 5% H<sub>2</sub>/Ar stream (18.6 mL/min) in a temperature range of 50 – 600°C (5°C/min).

#### 1.2.6 Absorbance UV/Vis spectroscopy

Absorbance UV/Vis spectroscopy was measured employing a UV-2600i UV/Vis spectrometer by Shimadzu equipped with an Integrating Sphere Attachment and a two-detector-setup. This means, the sample and the reference (BaSO<sub>4</sub>) were measured at the same time. All spectra were measured from 200 to 900 nm. The standard halogen and deuterium lamps provided by Shimadzu were used as light sources, switching at 300 nm. Prior to all measurements, a background using BaSO<sub>4</sub> was taken. The LabSolutions UV-Vis (Version 1.12) software was utilized for measurement control and data analysis.

#### 1.2.7 X-ray photoelectron spectroscopy (XPS)

The XPS measurements were carried out on an AXIS Supra+ device from Kratos Analytical Ltd. An Al-K $\alpha$  X-ray source with an energy of 1486.6 eV was used. Broad spectra were recorded in a range of 1200 - 0 keV in steps of 1 eV. Regional scans were acquired in steps of 0.1 eV and with five sweeps each (60 s scan time per sweep). The spectra were referenced to the C1s signal (284.7 eV). The data were analyzed using the ESCAPE software from Kratos and the casaXPS software.

#### 1.2.8 Pair distribution function (PDF)

*In-situ* high energy X-ray total scattering experiments for PDF analysis were conducted at beamline I15-1 at Diamond Light Source, Didcot (Uk) with an X-ray energy of 76.69 keV ( $\lambda = 0.161669 \text{ \AA}$ ). Scans were taken every 30 s with a beam size of 700 x 150  $\mu\text{m}$ , using a Perkin Elmer XRD 4343 CT flat panel detector. For the experiments, 5 mg of dried powder sample was filled in a 1.5 mm outer diameter (1.27 mm inner diameter) quartz glass capillary and held in place with quartz wool. The capillary was heated with a gas flow cell, that was connected to mass flow controllers from Alicat Scientific. The sample was first heated to 450 °C using a ramp of 5 °C/min and then held at 450 °C while filtered compressed air was flushed through the capillary with a flow rate of 10 ml/min. After more than an hour of calcination, no further changes were observed in the PDF. The gas was then switched to a 1:1 mixture of He and H<sub>2</sub> to reduce the sample using a total flow of 40 ml/min. Corrections and azimuthal integration of the 2D images were performed on the fly using the DAWN software package.<sup>[3]</sup>

Additional *ex-situ* measurements of samples after calcination, reduction, catalysis (spent) and a combination of reduction and later catalysis were conducted at the Petra III beamline P02.1 at DESY, Hamburg (Germany) using an X-ray energy of 59.8 keV (0.20733  $\text{\AA}$ ). Scans for each sample were collected over a time of 100 s using a Pilatus 2M CdTe area detector. Samples were filled in Kapton capillaries (1.05 mm outer and 1 mm inner diameter) right before the measurement to avoid oxidation during exposure to atmospheric conditions. A LaB<sub>6</sub> standard was measured for calibration of the detector distance and tilt, as well as instrumental resolution parameters. Corrections and azimuthal integration on *ex-situ* measurements were performed using the xpdtools software.<sup>[4]</sup> Later calculations of the PDFs were performed, using PDFGetX3<sup>[5]</sup>, using a  $Q_{\text{min}}$  of 0.4  $\text{\AA}^{-1}$  and a  $Q_{\text{max}}$  of 19.5  $\text{\AA}^{-1}$ , with a  $\Delta r$  of 0.01  $\text{\AA}$ .

Refinement of the PDFs were done using Diffpy-CMI on the range of 0.5 to 100 Å for the *ex-situ* data, and a range of 0.5 – 150 Å in the case of the *in-situ* data.<sup>[6]</sup>

### 1.3 Catalytic tests

The non-oxidative dehydrogenation (NOD) of methanol to dimethoxymethane (DMM) in the gas phase was carried out in a continuous flow fixed bed reactor as was reported in our previous publications.<sup>[1,2,7]</sup> Typically, 100 mg of the Ag/H $\beta$  catalysts were diluted with SiC (200 - 450 mesh size) and added to the stainless-steel tubular reactor. Unless otherwise stated, the catalyst was first reduced *in situ* at 450°C with a H<sub>2</sub> flow of 20 mL/min for 3 h and then cooled to room temperature under H<sub>2</sub> flow (10 mL/min). The reaction was carried out at 200 - 280°C and under previously optimized reaction conditions (1 atm, GHSV = 14549 mL/h\*g<sub>cat</sub>, n(CH<sub>3</sub>OH)/n(N<sub>2</sub>) = 0.24 (V/V)). For this purpose, methanol (0.008 mL/min) and N<sub>2</sub> (19.7 mL/min) were premixed in an evaporation chamber upstream of the reactor inlet and introduced into the catalyst bed (the gas mixture was stabilized over 1 h). All stainless-steel gas lines (inlet and outlet lines) and the evaporation chamber were heated to 140°C so that methanol and the products were in gaseous form. The reaction products (DMM, MF, and DME) and methanol were quantified using an online GC (Scion 456, Bruker, equipped with a flame ionization detector) connected to the reactor outlet. The selectivity to the respective products and the catalytic activity based on the methanol conversion were calculated using equations (1 – 3). The product selectivity (S<sub>p</sub> in %) to the respective product (DME, MF or DMM) and the methanol conversion (X in %) are calculated based on the molar concentration of carbon in each compound and an absolute calibration factor for each component was used. For example, DMM selectivity (S<sub>DMM</sub>) was calculated based on the molar carbon concentration in DMM (N<sub>DMM</sub>) divided by the sum of the molar carbon concentration of all compounds (N<sub>i</sub>) in the outlet stream, *i.e.*, methanol, DME, MF, and DMM (equation 1). N<sub>p</sub> is the molar carbon concentration in one of the products P (DME, MF or DMM).

The methanol conversion was accordingly calculated based on the molar carbon concentration of methanol in the outlet stream (N<sub>CH<sub>3</sub>OH</sub>) divided by the sum of the molar carbon concentration of all compounds in the outlet stream (N<sub>i</sub>) (equation 2, SI)

$$S_{DMM} = \frac{N_{DMM}}{\sum N_i} \cdot 100\% \quad (1)$$

$$S_p = \frac{N_p}{\sum N_i} \cdot 100\%$$

General formula:

$$X = \left[ 1 - \left( \frac{N_{CH_3OH}}{\sum N_i} \right) \right] \cdot 100\% \quad (2)$$

$$A = \frac{\left( \frac{F_{MeOH} \cdot X}{1000} \right)}{m_{cat}} \quad (3)$$

A denotes the catalytic activity, *i.e.*, the molar amount of methanol that is consumed per time and catalyst mass (mmol<sub>MeOH,conv</sub>/h/g<sub>cat</sub>) (equation 3). F<sub>MeOH</sub> denotes the inlet flow rate of methanol (mol/h) and m<sub>cat</sub> is the catalyst mass (g). The catalytic results are typically compared based on the selectivity and activity after 1500 min TOS, unless otherwise stated.

## 2 Characterization results

### 2.1 Physicochemical characterization

Table S 1. Physicochemical characterizations for Ag/H $\beta$  catalysts with varied Ag loading. The metal loading was quantified using ICP-OES analysis. Based on N<sub>2</sub>-physisorption analysis, the specific surface area ( $S_{BET}$ ) was quantified using the Brunauer-Emett-Teller (BET) method, and the total, micro-, and meso-pore volume ( $V_{total}$ ,  $V_{micro}$ ,  $V_{meso}$ , respectively) were quantified based on the t-plot method.

Sample	Ag loading (%)	$S_{BET}$ (m <sup>2</sup> /g)	$V_{total}$ (mL/g)	$V_{micro}$ (mL/g)	$V_{meso}$ (mL/g)
Ag1/H $\beta$	0.96	556	0.73	0.17	0.56
Ag5/H $\beta$	4.92	528	0.69	0.16	0.53
Ag20/H $\beta$	19.51	372	0.55	0.11	0.44

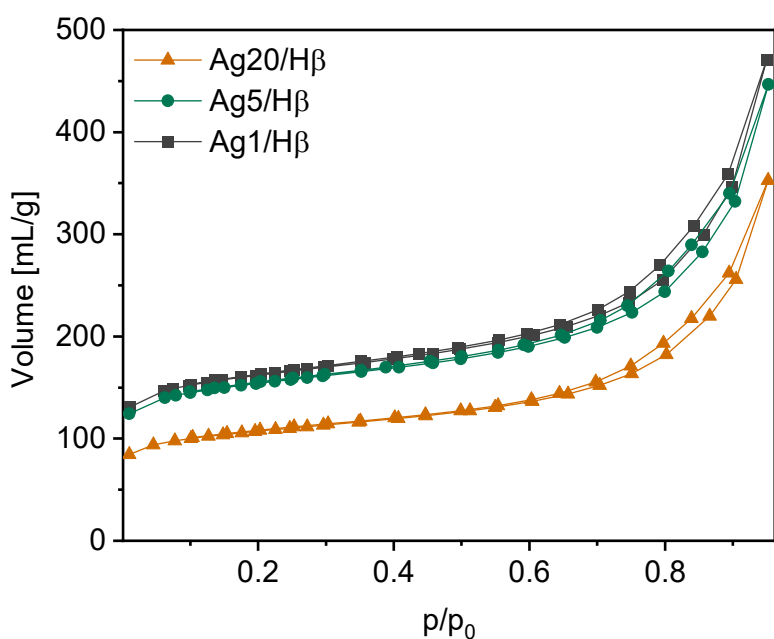


Figure S 1. N<sub>2</sub>-physisorption isotherms of the Ag/H $\beta$  catalysts.

## 2.2 XRD

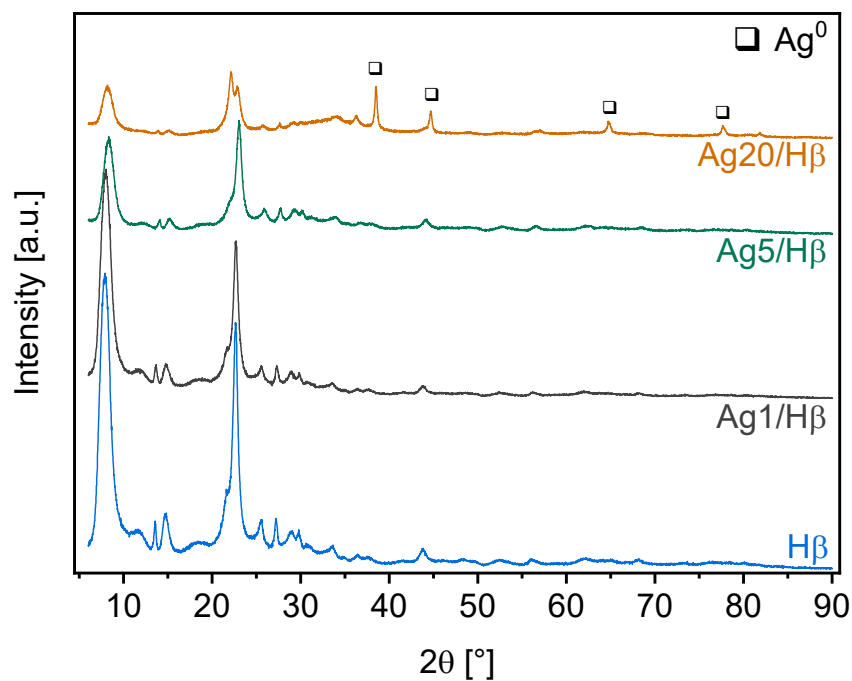


Figure S 2. XRD data of the calcined Ag/H $\beta$  catalysts with different Ag loadings, and the support H $\beta$  material. The diffractograms were collected on a benchtop D2 PHASER unit.

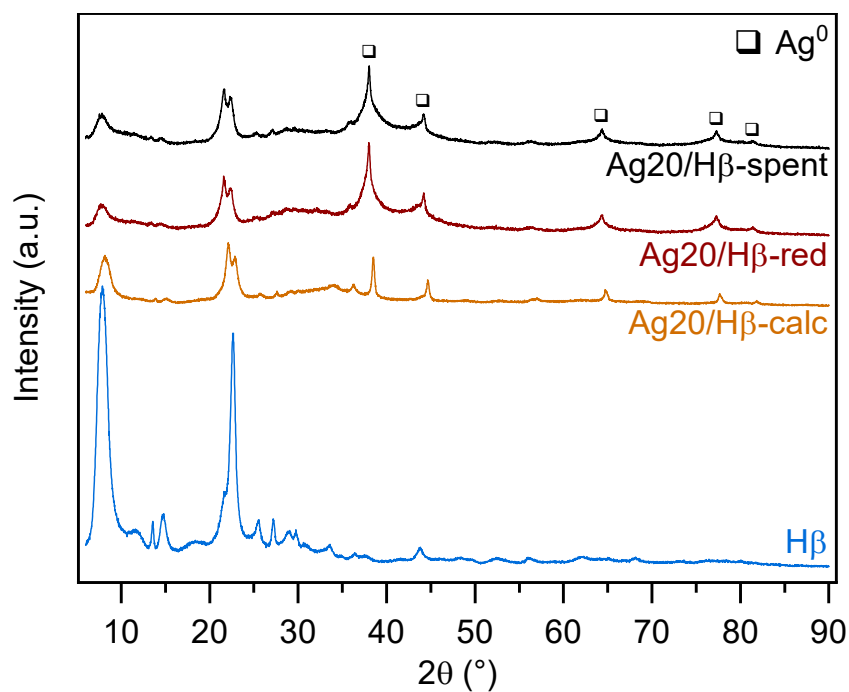


Figure S 3. XRD data of the Ag20/H $\beta$  catalyst synthesized by IWI after different treatments (calcination (= Ag20/H $\beta$ -calc), reduction (= Ag20/H $\beta$ -red), calcination and reaction (= Ag20/H $\beta$ -spent)), and the support H $\beta$  material. The diffractograms were collected on a benchtop D2 PHASER unit

### 2.3 PDF

PDF refinements of the *in-situ* data (Figure S 4) reveal the existence of a triclinic bulk  $\text{AgNO}_3$  (ICSD: 374) phase, for the precursor, which decomposes at 160 °C. As the PDF is not suitable for calculating particle sizes for a bulk phase, the particle size for  $\text{AgNO}_3$  was restricted to an upper limit of 500 Å. Apart from the silver salt and the support structure, no crystalline phase is observed until a sudden formation of metallic  $\text{Ag}^0$  (ICSD: 181730) particles is observed at 410 °C. The  $\beta$  zeolite is traditionally regarded to be a highly disordered structure which arises from a stacking disorder of the so-called periodic building units.<sup>[8]</sup> This is why the structural analysis of disordered zeolite structures remains a challenge to this day. In the case of  $\beta$  zeolite, it is assumed that this stacking disorder can be described as an intergrowth of the two zeolite polytypes A and B.<sup>[9]</sup> Refinements of the H $\beta$  zeolite in this study were conducted, using only the polytype A structure which is provided by the online Database of Zeolite Structures.<sup>[10]</sup> The structure was sufficient in describing the short-range order of the support. Together with the formation of Ag nanoparticles with a final size of 11 nm, a structural change appears in the signal of the H $\beta$  zeolite, which is indicated by the shift of two peaks from 2.63 and 3.06 Å to 2.78 and 3.21 Å respectively. For illustration of this, the signal of the support structure was isolated by subtracting the contribution of  $\text{AgNO}_3$  and Ag for the precursor and calcined data sets respectively (Figure S 5). This structural change in the short-range order can be explained by the incorporation of  $\text{Ag}^+$  ions into the crystal lattice of H $\beta$  zeolite during the calcination of the system. Refinement of the *in situ* PDF data suggests a small decrease in Ag particle size from 11 to 10 Å during pure  $\text{H}_2$  treatment of the sample at  $t = 160$  min (Figure S 4). This is accompanied by a decrease in the average domain size of the H $\beta$  zeolite. Even though this phenomenon is accompanied by a lattice contraction of Ag by 0.01 Å, this contraction alone cannot fully explain the observed decrease in size by 1 nm. A possible explanation could be the dynamic re-dispersion of Ag nanoparticles driven by surface hydrogen. It has been shown that hydrogen spillover and reverse spillover can significantly influence the dynamic evolution and migration of nanoparticles.<sup>[11]</sup> Furthermore, the spillover phenomenon has been predicted to occur on zeolite structures.<sup>[12]</sup> In addition, lattice strain is known to cause significant linear Lorentzian broadening of PDF peaks, which can lead to inaccurate estimates of crystallite domain sizes.<sup>[13]</sup> However, strain also typically results in an increase in atomic displacement parameter (ADP) values, neither of which is observed in this case, making lattice strain an unlikely explanation. While further research is required to gain deeper insights into this hypothesis, the PDF data clearly indicate a sort of restructuring of the metal particles, as well as the support structure.

Refinements for the *ex-situ* measurements can be seen in Figure S 6 and Figure S 7. Refinements for the reduced, spent and the reduced spent catalyst show little differences, while for the calcined catalyst some discrepancies between experimental and theoretical structure are observed in the short-range order, see difference curve in Figure S 6A. Such an observation could be explained by the restructuring of metal nanoparticles inside the zeolites pore system, leading to a less distorted support structure.

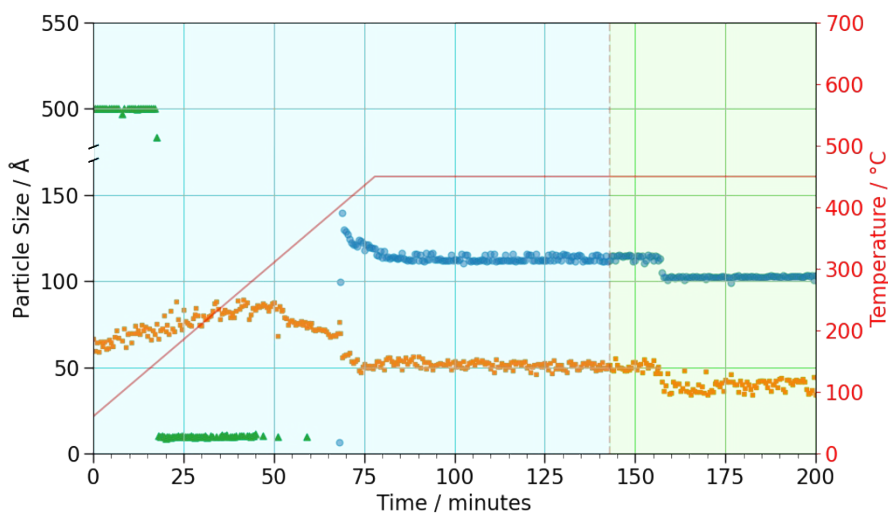


Figure S 4. Resulting particle size of the refinement of in-situ PDF data from I15-1.  $\text{AgNO}_3$  (green triangles), metallic Ag (blue dots) and  $\text{H}\beta$  zeolite (orange squares).  $\text{AgNO}_3$  shows a bulk particle size which is limited to 500 Å by the refinement, while the  $\text{H}\beta$  zeolite appears to have a very small crystalline domain sizes, which can be explained by the stacking fault character of the zeolite structure. The blue and green backgrounds illustrate the time frame of calcination and reduction, respectively

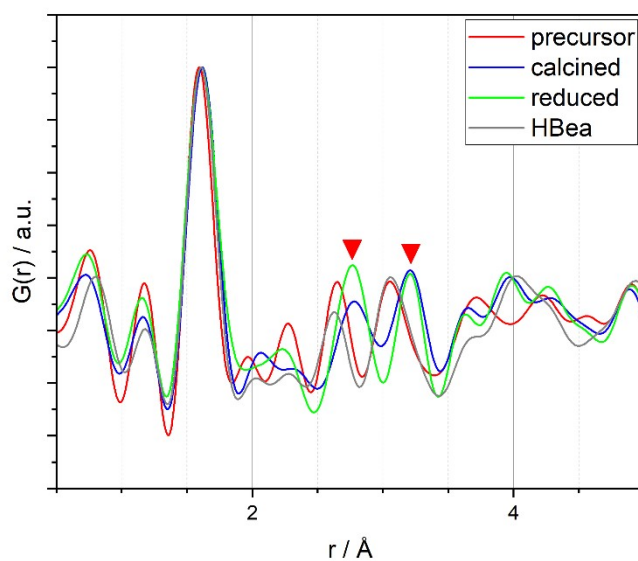


Figure S 5. Difference curves of the refinements of the precursor (red) with  $\text{AgNO}_3$ , the calcined (blue) and reduced (green) catalyst with Ag nanoparticles. The gray line shows a measurement of unloaded dealuminated  $\text{H}\beta$  zeolite. The curve of the precursor shows a similar pattern to the pristine support. Structural changes of the  $\text{H}\beta$  zeolite during calcination becomes evident, by the shift of two distances, highlighted by the red triangles. Structural changes keep persisting during reduction. Data was collected at the I15-1 beamline of Diamond Light Source and normalized to its maximum intensity.

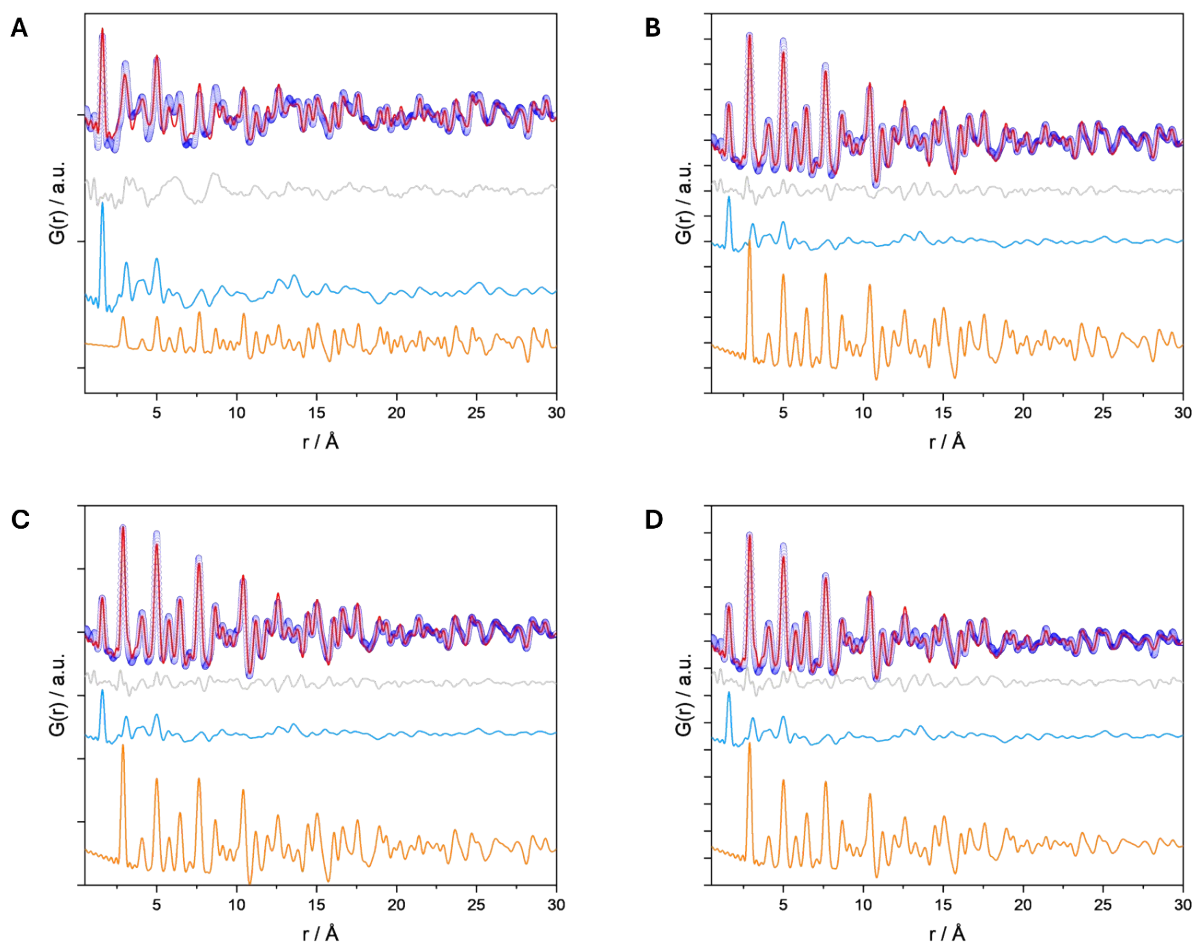


Figure S 6. Refinements of PDFs of the calcined catalyst (A), the reduced catalyst (B), the catalyst after usage (C) and the catalyst after a reduction and later usage (D). Blue dots indicate the observed data set while the calculated PDF is shown in red. The resulting difference curve is shown in green. The light blue line shows the contribution of the fitted theoretical H $\beta$  zeolite phase and the orange line the contribution of Ag nanoparticles. Data was collected at the P02.1 beamline of DESY.

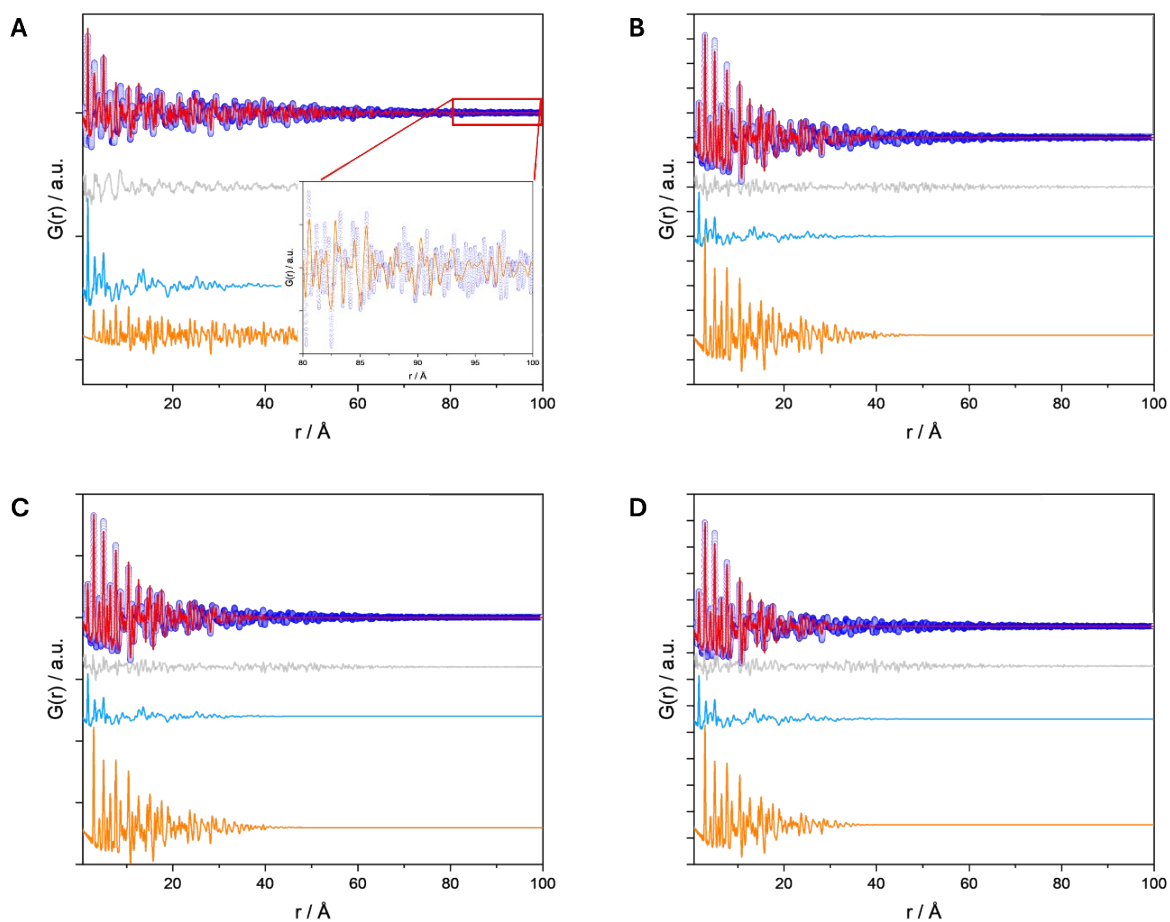


Figure S 7. Same refinements of PDFs as shown in Figure S 6, but up to 100 Å to illustrate the long-range order. The area of 80–100 Å is magnified in the case of the calcined sample to highlight the refinement of the long-range order by the Ag phase.

## 2.4 H<sub>2</sub>-TPR

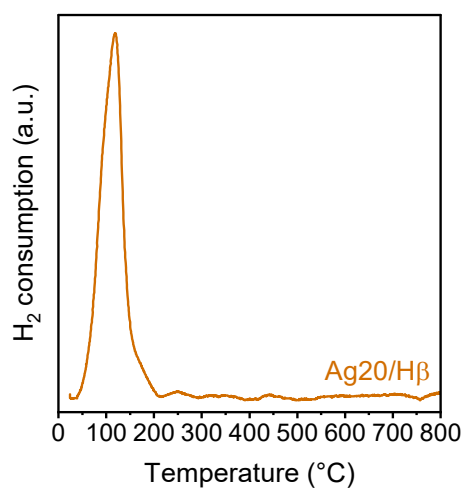


Figure S 8. H<sub>2</sub>-TPR results of the calcined Ag<sub>20</sub>/Hβ catalyst. A baseline correction of the data was performed.

## 2.5 UV/Vis

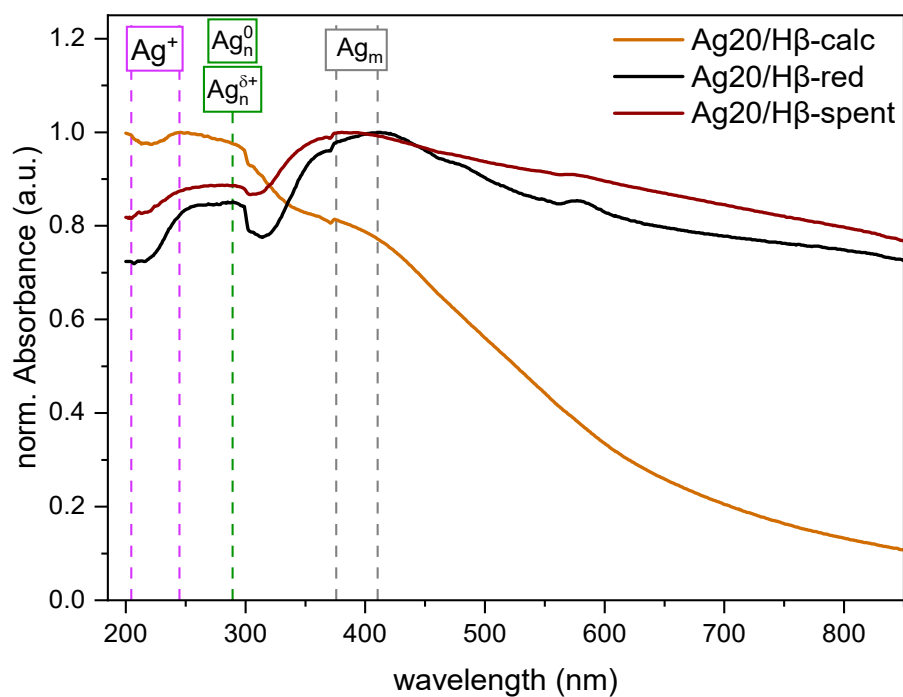


Figure S 9. Normalized UV/Vis absorbance spectra of the calcined, reduced and spent Ag<sub>20</sub>/Hβ catalysts. The UV/Vis absorbance spectrum of the unloaded Hβ support was used as background.

## 2.6 Thermogravimetric analysis

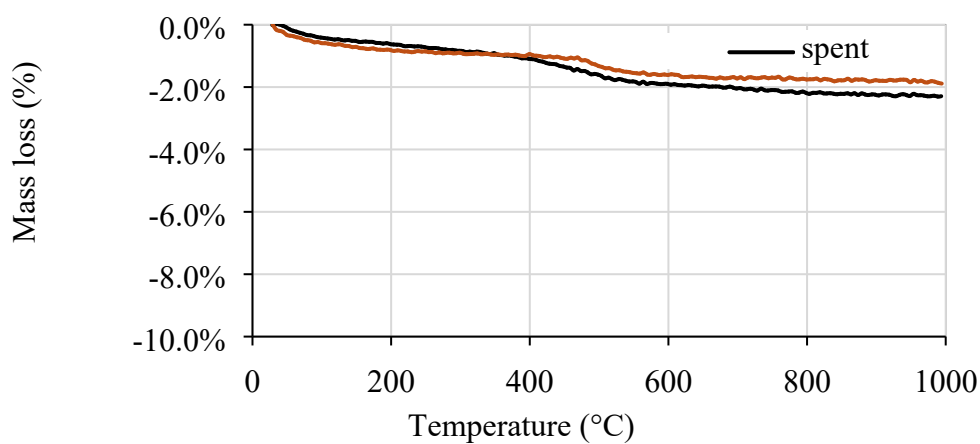


Figure S 10. TG analysis of the calcined and spent Ag<sub>20</sub>/Hβ catalyst in air.

## 2.7 XPS

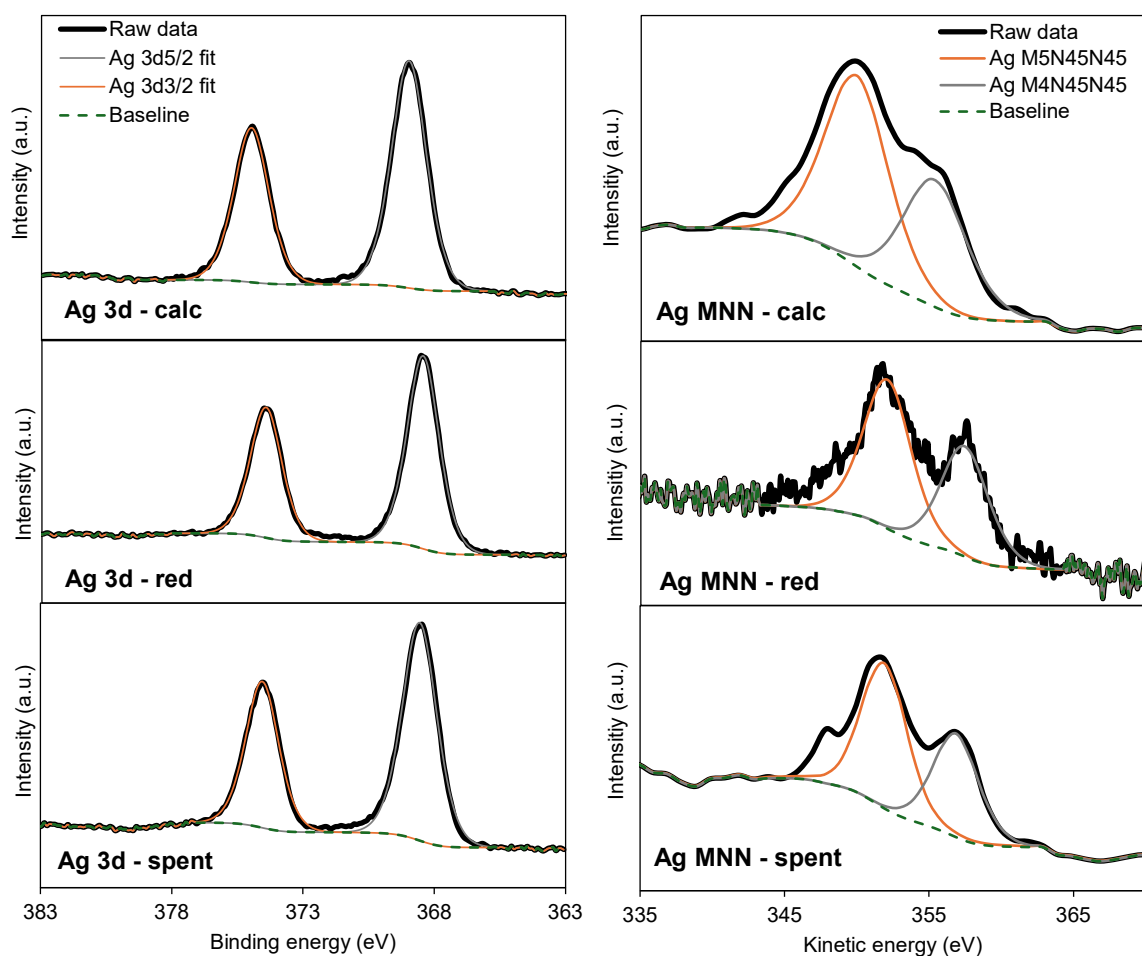


Figure S 11. XPS detailed regions of Ag 3d and Ag MNN of the calcined, reduced and spent Ag<sub>20</sub>/H $\beta$  catalysts.

Calculation of the Auger parameters (AP) according to:

$$\text{AP} = \text{binding energy (Ag } 3d_{5/2}) + \text{kinetic energy (KE) (Ag MNN)}.^{[14]}$$

Table S 2. XPS results and calculated AP for Ag<sub>20</sub>/H $\beta$  after calcination (=calc), reaction (=spent) and reduction (=red).

	Ag <sub>20</sub> /H $\beta$ -calc	Ag <sub>20</sub> /H $\beta$ -spent	Ag <sub>20</sub> /H $\beta$ -red
<b>Position (BE) Ag 3d<sub>5/2</sub> (eV)</b>	369.0	368.6	368.4
<b>Position (KE) Ag M4N45N45 (eV)</b>	355.4	356.9	357.5
<b>AP (M4)</b>	<b>724.3</b>	<b>725.5</b>	<b>726.0</b>

### 3 Catalytic results in the NOD of methanol to DMM

#### 3.1 Screening of Ag loading

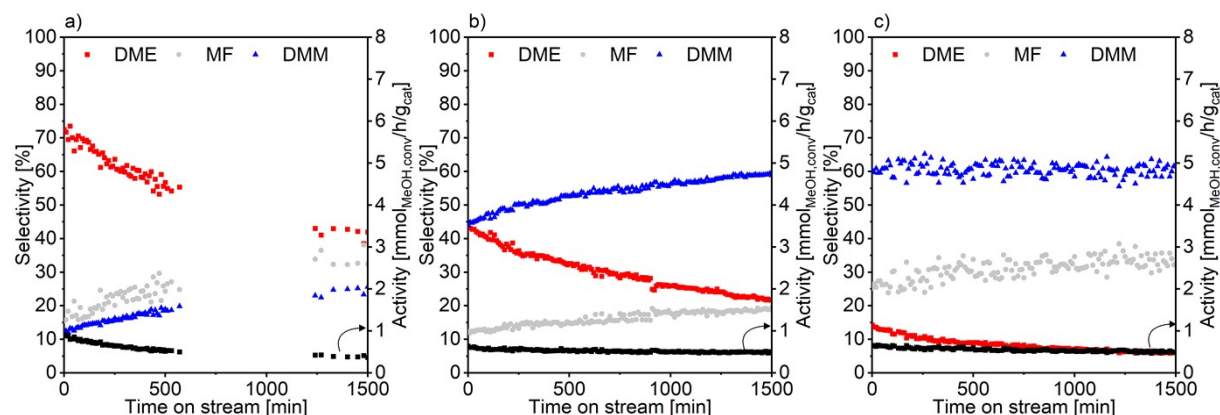


Figure S 12. Catalytic results in the NOD of methanol to DMM with a) 1, b) 5, and c) 20 wt.% Ag loaded Ag/H $\beta$  catalysts. Reaction conditions: 1 atm, GHSV = 14549 mL/h $\cdot$ g $_{\text{cat}}$ ,  $T = 200^\circ\text{C}$ , 0.1 g of catalyst diluted with 0.9 g of SiC,  $n(\text{CH}_3\text{OH})/n(\text{N}_2) = 0.24$ ,  $\text{N}_2$  flow rate = 19.7 mL/min, in situ reduction prior to reaction ( $450^\circ\text{C}$ , 3 h,  $\text{H}_2$  flow rate = 20 mL/min).

#### 3.2 Screening of reaction temperature

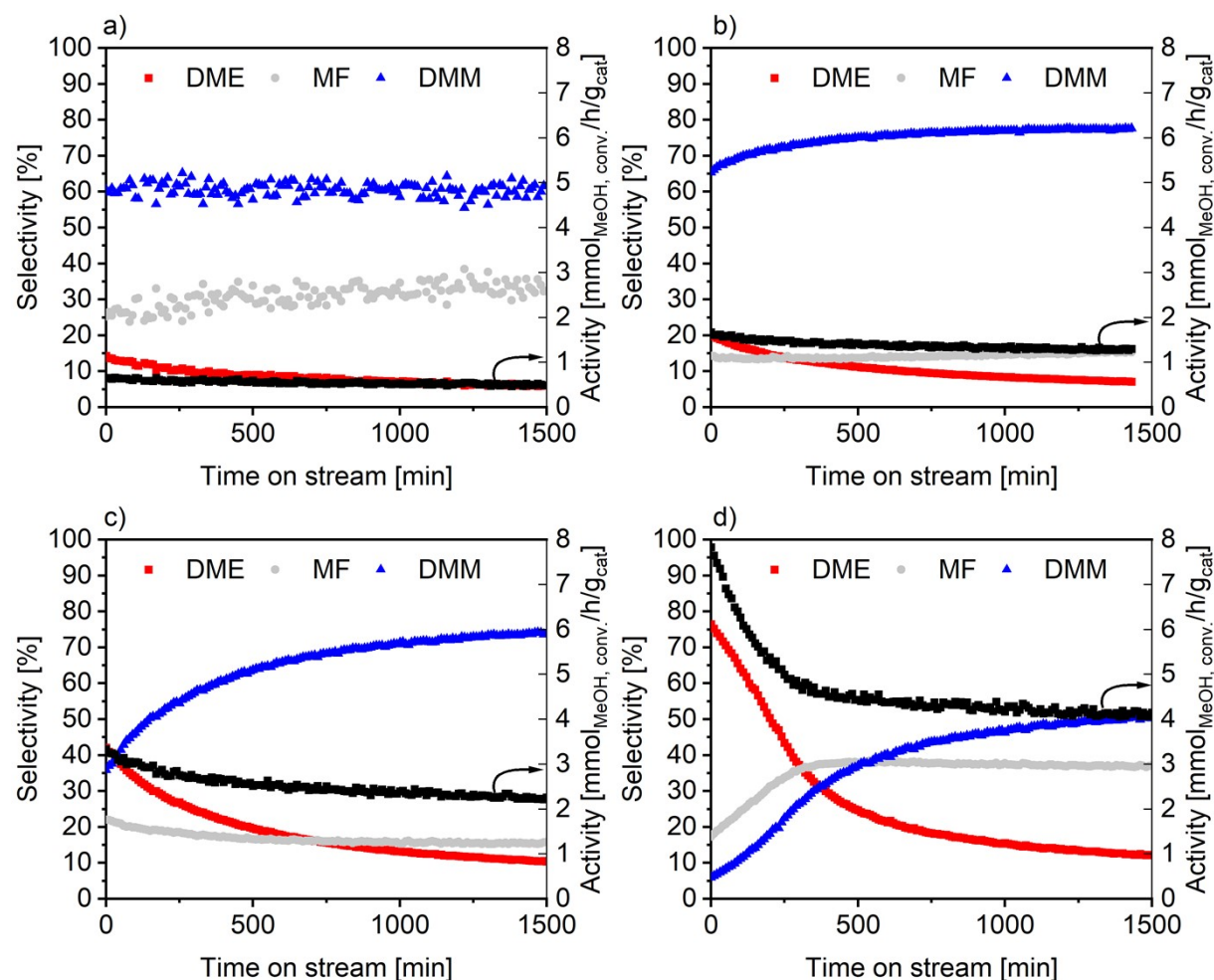


Figure S 13. Catalytic results for the NOD of methanol to DMM over Ag<sub>20</sub>/H $\beta$  catalyst at reaction temperatures of a) 200°C, b) 220°C, c) 240°C, d) 280°C. Reaction conditions: 1 atm, GHSV = 14549 mL/h $\cdot$ g $_{\text{cat}}$ , 0.1 g of catalyst diluted with 0.9 g of SiC,  $n(\text{CH}_3\text{OH})/n(\text{N}_2) = 0.24$ ,  $\text{N}_2$  flow rate = 19.7 mL/min, in situ reduction prior to reaction ( $450^\circ\text{C}$ , 3 h,  $\text{H}_2$  flow rate = 20 mL/min).

### 3.3 Screening of pre-treatment (calcination, reduction)

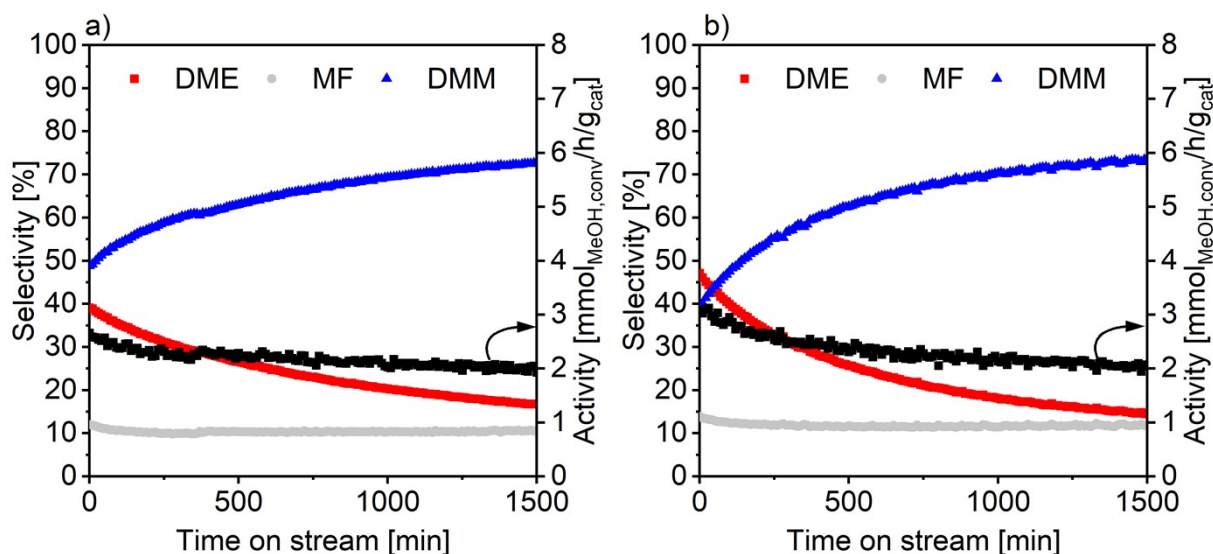


Figure S 14. Catalytic results in the NOD of methanol to DMM over the Ag<sub>20</sub>/H $\beta$  catalyst which was a) calcined or b) in situ reduced prior to the reaction. Reaction conditions: 1 atm, GHSV = 14549 mL/h\**g*<sub>cat.</sub>, T = 240 °C, 0.1 g of catalyst diluted with 0.9 g of SiC, n(CH<sub>3</sub>OH)/n(N<sub>2</sub>) = 0.24, N<sub>2</sub> flow rate = 19.7 mL/min, optional in situ reduction prior to reaction (450 °C, 3 h, H<sub>2</sub> flow rate = 20 mL/min).

## 4 References

- [1] C. Mebrahtu, R. Sun, C. Gierlich, R. Palkovits, *Appl. Catal., B* **2021**, 287, 119964.
- [2] N. Simitsis, C. Mebrahtu, R. Palkovits, *ChemCatChem* **2024**, 16, e202301704.
- [3] J. Filik, A. W. Ashton, P. C. Y. Chang, P. A. Chater, S. J. Day, M. Drakopoulos, M. W. Gerring, M. L. Hart, O. V. Magdysyuk, S. Michalik et al., *J. Appl. Crystallogr.* **2017**, 50, 959.
- [4] C. J. Wright, X. D. Zhou, *J. Synchrotron Radiat.* **2017**, 24, 506.
- [5] P. Juhás, T. Davis, C. L. Farrow, S. J. L. Billinge, *J. Appl. Crystallogr.* **2013**, 46, 560.
- [6] P. Juhás, C. L. Farrow, X. Yang, K. R. Knox, S. J. L. Billinge, *Acta Crystallogr. A: Found. Adv.* **2015**, 71, 562.
- [7] R. Sun, C. Mebrahtu, J. P. Hofmann, D. Bongartz, J. Burre, C. H. Gierlich, P. J. C. Hausoul, A. Mitsos, R. Palkovits, *Sustain. Energy Fuels* **2021**, 5, 117.
- [8] T. Willhammar, X. Zou, *Z. Kristallogr. – Cryst. Mater.* **2013**, 228, 11.
- [9] M. M. Martínez-Iñesta, I. Peral, T. Proffen, R. F. Lobo, *Microporous Mesoporous Mat.* **2005**, 77, 55.
- [10] C. Baerlocher, L. B. McCusker, "Database of Zeolite Structures", can be found under <https://www.iza-structure.org/databases/>.
- [11] R.-P. Zhang, B. He, X. Liu, A.-H. Lu, *J. Am. Chem. Soc.* **2023**, 145, 25834.
- [12] S. Lee, H. Kim, R. Ryoo, J. Y. Park, M. Choi, *Nano Res.* **2022**, 15, 10357.
- [13] J. Beyer, N. Roth, B. Brummerstedt Iversen, *Acta Crystallogr. A: Found. Adv.* **2022**, 78, 10.
- [14] A. M. Ferraria, A. P. Carapeto, A. M. Botelho do Rego, *Vac.* **2012**, 86, 1988.